



Morphology and texture characterization of grains in laser welding of aluminum alloys

Qihan Gao¹ · Cheng Jin¹ · Zhibin Yang¹

Received: 6 July 2020 / Accepted: 13 October 2020 / Published online: 6 January 2021
© International Institute of Welding 2021

Abstract

Grain morphology and texture of welds significantly affect the properties of the corresponding joint. It is very important to determine how heat and grain growth during welding correlate. Our studies involved both experiments and multi-scale numerical modeling. The laser welding temperature distribution was studied by the macroscopic finite element method. The grain growth and morphology evolution under different heat input conditions were calculated by the Monte Carlo method at the mesoscale. The relationship between heat flow distribution and grain orientation was established. Results of electron backscattered diffraction (EBSD) were compared to those obtained by numerical modeling. The welding heat input affected the heat flow distribution and the shape of the molten pool, which, in turn, influenced grain morphology and crystal orientation.

Keywords Laser welding · Finite element · Monte Carlo · Grain growth · Heat flow · Crystal orientation

1 Introduction

Among the different fusion welding methods used on Al-based alloys, laser welding offers higher speed, increased penetration depth, and smaller deformation, and has been used in increasing numbers of applications in recent years [1]. The grain mesostructure of the welded Al alloys is one of the most important factors affecting welded joint functionality and long-term performance.

Grain growth during welding solidification have been studied over many years since the pioneering work of F. Matsuda [2], G.J. Davies [3] and W.F. Savage [4] et al. It is well accepted that the weld pool shape determined

by the thermal conditions has a critical influence on the evolution of weld grains. Owing to the recent development in numerical modeling techniques, the solidification of weld can be studied more efficiently and accurately. The numerical tools are becoming more and more important to quantitatively characterize the weld microstructure and even the joint performance. Common numerical techniques for non-isothermal grain growth calculations include cellular automaton (CA) and Monte Carlo (MC) methods. CA method models the evolution of grain structure by applying local physical rules at the cellular level. CA simulations are easy to link to the macroscale modeling methods such as finite element (FE) and are widely implemented to model the grain evolution in castings and welding processes [5, 6]. However, being a deterministic method, CA-based simulations do not take into account dendrite branching [7]. Dendrite branching is important because their presence often leads to the formation of the grains slightly different from those observed typically.

MC-based simulations are probabilistic in nature and they model the grain structure evolution by tracking grain boundary movements, which occur due to the grain boundary energy decrease. Wei et al. [8] used MC simulations to analyze how different welding speeds affect the growth and evolution of grains. They modeled the equiaxed and columnar grains in the fusion and heat-affected zones (FZ and HAZ, respectively). Rodgers et al.

Recommended for publication by Commission IX - Behaviour of Metals Subjected to Welding

✉ Cheng Jin
jincheng@126.com

Qihan Gao
934377143@qq.com

Zhibin Yang
yangzhibinbk@163.com

¹ Department of Welding Technology and Engineering,
Dalian Jiaotong University, Dalian,
People's Republic of China

[9] established a three-dimensional model to simulate grain growth during welding using Potts model based on the MC algorithm. The process of grain growth in the FZ and HAZ is controlled by the moving speed and the parameters of the weld pool and compared them with the optical microscope observation. Good agreement in the grain morphology has been achieved. However, optical microscope observations can only give information on grain morphology but not the grain orientation, which also have critical influence on the macroscopic properties of the joint. Few researchers [10, 12] have reported simultaneous experimental and theoretical studies on both the grain morphology and orientation of laser-welded aluminum alloys.

Therefore, we used both numerical and experimental techniques to study the grain growth during the laser welding of an aluminum alloy. The macroscopic temperature field and the heat flow distribution during the welding process were studied by FEM. The mesoscopic grain growth of the weld under certain welding parameters was assessed using the MC method. Theoretical grain texture characterization was also performed and compared with the corresponding experimental measurements.

2 Experiments and models

2.1 Welding experiments

A 3-mm-thick AA1060 aluminum alloy plate was used and the composition is shown in Table 1.

The welding experiment was carried out using an IPG YSL-6000 fiber laser system (maximum power of which is 6000 W) equipped with a KUKA-30HA high-precision robot. Experiments were performed at different laser powers and welding speeds (see Table 2) on the premise of ensuring good weld formation. 99.99% Ar at 25 L/min flow rate served as the shielding gas.

$10 \times 10 \times 3$ mm pieces were cut from the welded samples from the center of the weld seam using electro-discharge machining. The top surfaces of these samples were first polished mechanically using $0.05 \mu\text{m}$ Al_2O_3 powder and then electro-polished at 15 V for 5 min in 25% perchloric acids (HClO_4) ethanol solution. The analysis area was located in the center of the weld line and was large enough to simultaneously cover the FZ, HAZ, and partial base metal of the sample. The x -axis was defined to be parallel to the welding direction while the y -axis was in the plane of

Table 1 Chemical composition of AA1060 alloy (wt%)

Elements	Si	Fe	Cu	Mn	Others	Al
Content	0.11	0.36	0.03	0.036	0.02	Balance

Table 2 Welding speed and laser power values used in experiments

Cases	Power (W)	Speed (m/min)	Heat input (J/mm)
Case I	2000	1	120
Case II	3500	2.4	87.5
Case III	5000	4	75
Case IV	5800	6	58

the sample but perpendicular to the welding direction. The scanning step was 10–20 μm . Channel 5 software package developed by HKL Inc. was used for data analysis.

2.2 Macroscopic modeling

A 3D heat transfer model was used to calculate the macroscopic temperature and heat flux fields using FE method. The properties of the AA1060 aluminum alloy used for the simulations are shown in Table 3.

A heat source model [13], which combined a Gaussian surface and a cone body heat source models (described by equations (1) and (2), respectively), was used for laser heat input simulation during the welding process (see Fig. 1).

$$q(r) = \frac{3\eta\phi_{sur}}{\pi R_0^2} \exp\left(-\frac{3r^2}{R_0^2}\right) \quad (1)$$

where r is the distance from the center of the heat source, R_0 is the effective heating radius, η is the thermal efficiency, and ϕ_{sur} is the surface source part of applied laser power.

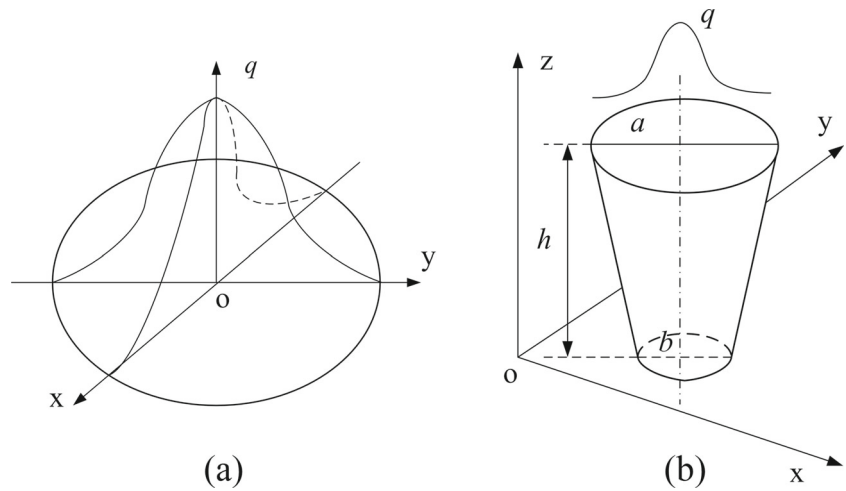
$$\begin{cases} q(r, z) = \frac{9\eta\phi_{vol}e^3}{\pi(e^3-1)} \cdot \frac{\exp\left(-\frac{3r^2}{r_0^2(z)}\right)}{h \cdot (a^2+ab+b^2)} \\ r_0(z) = a - \frac{(a-b) \cdot z}{h} \end{cases} \quad (2)$$

where ϕ_{vol} is the volume source part of applied laser power; e is a natural constant; r is the distance from the cone axis; z is the distance from the top surface of the weld; h is depth of the heat source; a and b are the effective heating radii of the upper and lower surfaces of the cone body, respectively; and $r_0(z)$ is the heating radius of any horizontal cross-section of the cone body.

Table 3 Properties of AA1060 aluminum alloy used for the FE model [11]

Variables	Value
Thermal conductivity, W/(m K)	222
Specific heat, J/(kg K)	904
Density, kg/m^3	2700
Melting latent heat, J/kg	3.95×10^5
Solidus temperature, K	916
Liquidus temperature, K	930

Fig. 1 Gaussian surface (a) and cone body (b) heat source models



A fixed time incrementation was adapt to facilitate the link between FE and MC simulations, which is explained in detail in the next section.

2.3 Grain growth model

The grain growth was simulated using the kinetic Monte Carlo (kMC) algorithm, which is based on the Potts model [14]. This paper emphasizes the relationship between the real-time and MC time (t_{MCS}), which is critical to link the macroscopic simulations with the mesoscopic ones [15]. According to grain boundary migration model (GBM), their relationship can be expressed by Eq. (3) [7]:

$$(t_{MCS})^{2n_1} = \left(\frac{L_0}{K_1\lambda}\right)^2 + \frac{4\gamma AZV_m^2}{K_1^2\lambda^2 N_a^2 h} e^{\Delta S_a/R} \sum_{i=1}^m [\Delta t_i \cdot \exp(-\frac{Q}{RT_i})] \quad (3)$$

where L_0 is the initial grain size; λ is the grid spacing; K_1 and n_1 are the constants obtained through the thermostatic simulation and regression analysis; A is the probability of adaptation; Z is the average atomic number per unit area of the grain boundary; V_m is the atomic molar volume; γ is the grain boundary energy; and Q is the activation energy of grain growth; ΔS_a is the activation entropy, N_a , h and R are the Avogadro, Planck and the gas constants, respectively; and T_i is the mean temperature in a small real-time interval, Δt_i . Mishra [7] pointed out that the influence of the initial grain size, L_0 , on the simulation results cannot be neglected. The initial grain size in the MC simulations is not the same as the measured initial grain size of the material. The initial grain size in the modeling is a dimensionless quantity, and its value is set equal to the grid spacing, λ . Therefore, the average grain size L can be expressed as:

$$L = \lambda + K_1 \times \lambda \times (t_{MCS})_1^n \quad (4)$$

By combining Eqs. (3) and (4), the MC simulation time and real-time corrected in the GBM model can be expressed as follows [7]:

$$t_{MCS} = \left\{ \frac{1}{K_1\lambda} \left[\frac{4\gamma AZV_m^2}{K_1^2\lambda^2 N_a^2 h} e^{\frac{\Delta S_a}{R}} \sum_{i=1}^m [\Delta t_i \cdot \exp(-\frac{Q}{RT_i}) + L_0^2] - \frac{1}{K_1} \right]^{\frac{1}{n_1}} \right\} \quad (5)$$

T_i can be obtained at a certain time interval Δt_i from the macroscopic temperature field calculation. Therefore, the MC time is linked with the real-time in macroscopic simulation. The rest of the model parameters can be obtained through the corresponding review and regression analysis. Numerical values of all parameters used in this paper are presented in Table 4. For more details about the kMC algorithm, please refer to Refs. [16–21].

Table 4 Parameters used for the mesoscopic simulations [21]

Variables	Value
Model constant, K_1	0.141
Model constant, n_1	0.48
Average number per unit area, Z (atoms/m ²)	1.1×10^{19}
Avogadro’s number, N_a (mol ⁻¹)	6.02×10^{23}
Accommodation probability, A	1.0
Atomic molar volume, V_m (m ³ /mol)	1.0×10^{-5}
Activation enthalpy for grain growth, Q (J/mol)	1.42×10^5
Activation entropy, ΔS_a (J/mol/K)	2.45
Gas constant, R (J/mol/K)	2.0
Planck’s constant, h (J s)	6.624×10^{-34}
Grain boundary energy, γ (J/m ²)	0.324
Initial grid spacing, λ (μ m)	10
Initial grain size, L_0 (μ m)	40

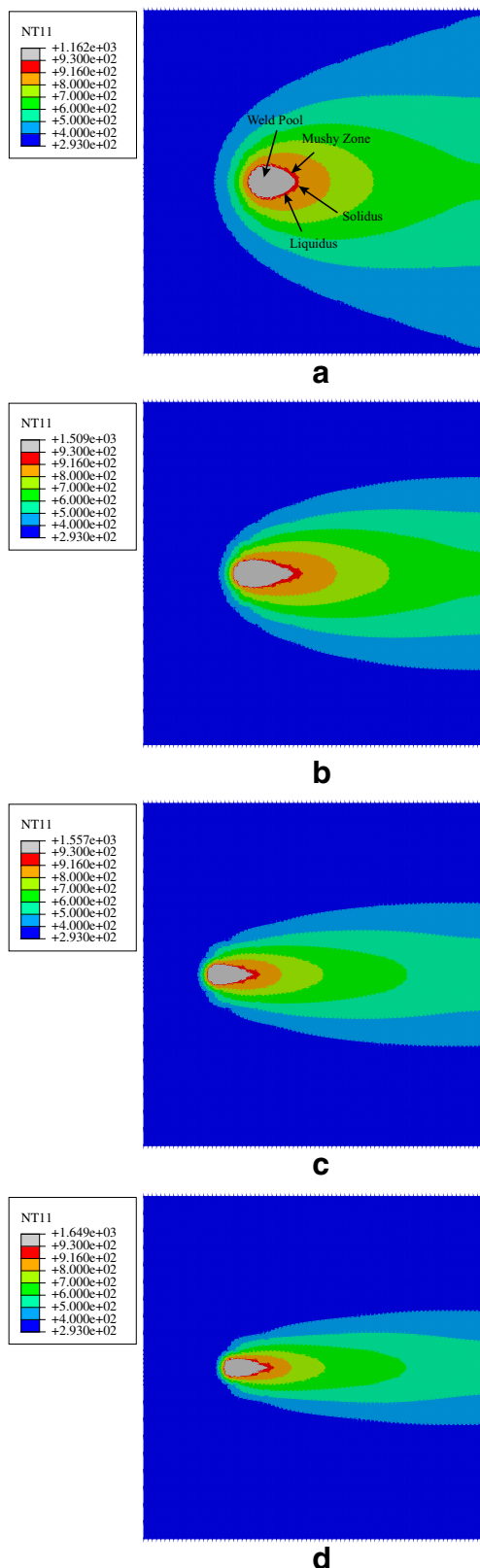


Fig. 2 Macroscopic temperature field. Corresponding heat inputs are **a** 120 J/mm, **b** 87.5 J/mm, **c** 75 J/mm and **d** 58 J/mm

3 Results and discussion

3.1 Macroscopic simulations

Temperature field and molten pool shape The temperature field results are shown in Fig. 2. The gray and red areas represent the molten pool and the partially melted metal (mushy zone), respectively.

As the heat input decreases, the size of the weld pool shrinks and the aspect ratio increases. Table 5 compares the weld geometry between experimental and numerical simulation results.

The shape and boundary directions of the weld pool can be used to qualitatively analyze grain growth. In general, grain solidification occurs perpendicular to the trailing edge of the weld pool because this direction has a maximum temperature gradient and fastest heat transfer [22]. At a certain heat input, the weld adopts a teardrop or elliptical shape at high and low welding speeds, respectively. Since the trailing boundary of a teardrop-shaped weld pool is essentially straight, the columnar grains are also straight, which helps them to grow perpendicular to the boundary. Because the trailing boundary of an elliptical weld pool is curved, the columnar grains are also curved.

Analysis of heat flow distribution can provide insights on the mechanism of grain morphology change during the growth. The direction of the heat flow is perpendicular to the weld pool and mushy zone boundary, which makes the straight columnar grains point toward the weld centerline at higher welding speed, while curved columnar grains point in the welding direction and mushy zone boundary at lower welding speed.

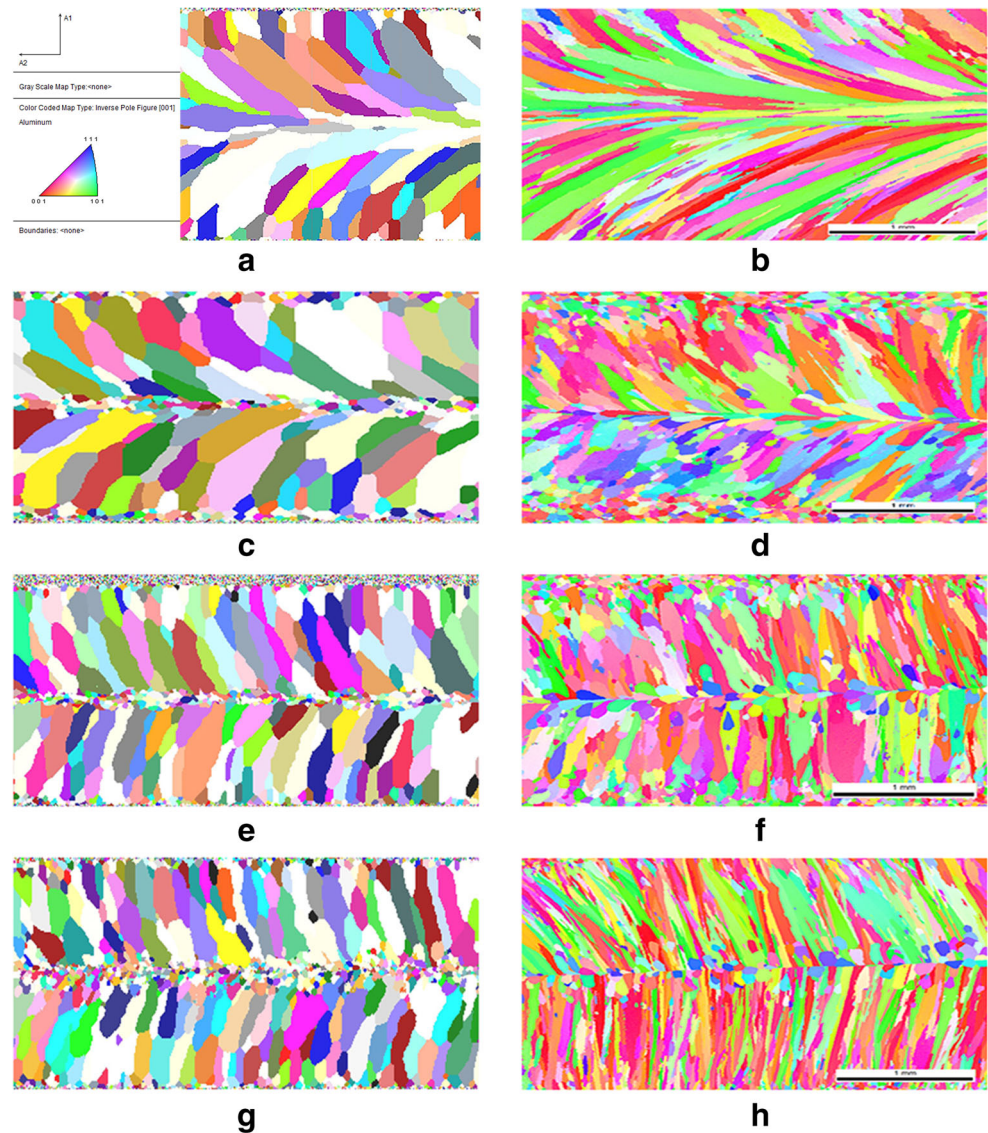
3.2 Mesoscopic simulations

Grain morphology and distribution Mesoscopic simulations provide insights into the columnar and equiaxed grain growth under different heat inputs. Grain structure and morphology of the top surface of the weld obtained by both simulation and experimental methods show good agreement (see Fig. 3). The morphology of the columnar grains

Table 5 Comparison between experimental and numerical simulation results of weld geometry

Cases	Weld top width (mm)		Weld bottom width (mm)	
	Simulation	Experiment	Simulation	Experiment
Case I	3.6	3.5	3.0	2.8
Case II	3.2	2.9	2.5	2.4
Case III	2.5	2.3	1.5	1.6
Case IV	2.1	1.8	0.8	1.0

Fig. 3 Comparison of KMC simulation results (a, c, e, g) with the EBSD results (b, d, f, h). a, b 120 J/mm, c, d 87.5 J/mm, e, f, 75 J/mm, and g, h 58 J/mm



changes from the curved to the straight one as the pool shape change from elliptical to teardrop one. The columnar grains become thinner as the heat input decreases. This is because the welding speed also affects the columnar crystal growth. High-temperature residence time is an important parameter of the welding thermal cycle. Fast welding speeds will shorten high-temperature residence time, which will result in insufficient heating of the columnar grains and, as a consequence, their inability to adequately expand grain boundaries.

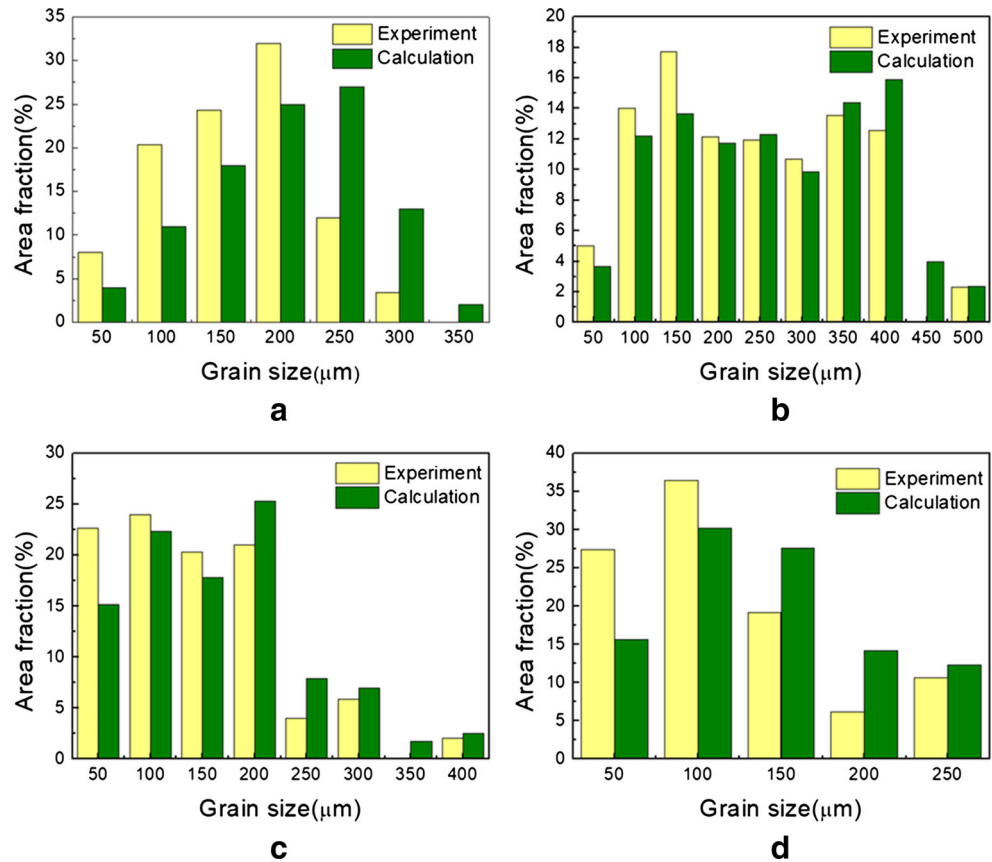
The equiaxed grains begin to appear in the weld centerline at 87.50 J/mm heat input. The number of equiaxed grains increases as the heat input continues to decrease. Nucleation and growth of the equiaxed grains follow heterogeneous mechanism [23]. These heterogeneous nucleation points only exist near the cooler pool boundary, which is located mostly in the mushy zone [24]. The mushy zone is

associated with the trailing portion of the weld pool. The area of the mushy zone is defined by the metal liquidus and solidus. The temperature gradient becomes smaller as the heat input decreases. Therefore, the ratio of the mushy zone area to the molten pool is inversely proportional to the heat input (see Fig. 2). As the heat input decreases, the temperature gradient (G) at the end of the molten pool decreases while the solidification rate (R) increases. Thus, G/R is expected to decrease, which is critical for the formation of the equiaxed grains.

The grain size distribution and the average grain size obtained by EBSD and numerical simulation are illustrated and compared in Figs. 4 and 5 respectively.

Both the experimental measurement and the numerical simulation give the relatively consistent distribution of grain size. Generally, the grain size reduces as the heat input decreases. However, there is an abnormal rise in case II

Fig. 4 Grain size distribution obtained by EBSD and KMC simulation for heat input **a** 120 J/mm, **b** 87.5 J/mm, **c** 75 J/mm and **d** 58 J/mm



(heat input is 87.5 J/mm). It obtained the largest average grain size among the four cases. It is worth noting that the grain morphology in case II is on the stage of transition from curved to straight. The straight columnar grains grow more easily than curved grain because of the competitive growth of columnar grains. Therefore, the larger grain size was obtained in case II even though the heat input and weld width are lower than that in case I.

It could also be found that the average grain size obtained from numerical simulation is slightly larger than that of experimental measurement in the four cases. This is because that the weld pool is assumed to be at steady state in the numerical calculations and the effect of fluid flow on the grain growth is neglected. The fluid flow in the weld pool can hinder the growth of columnar grains, which makes the grain size calculated slightly larger than that of the EBSD observation.

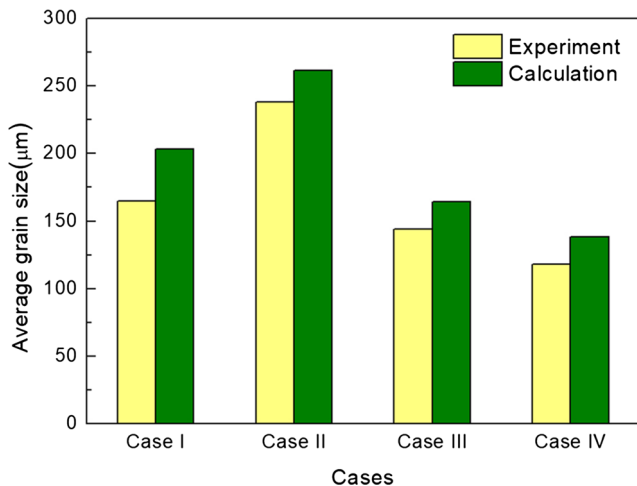
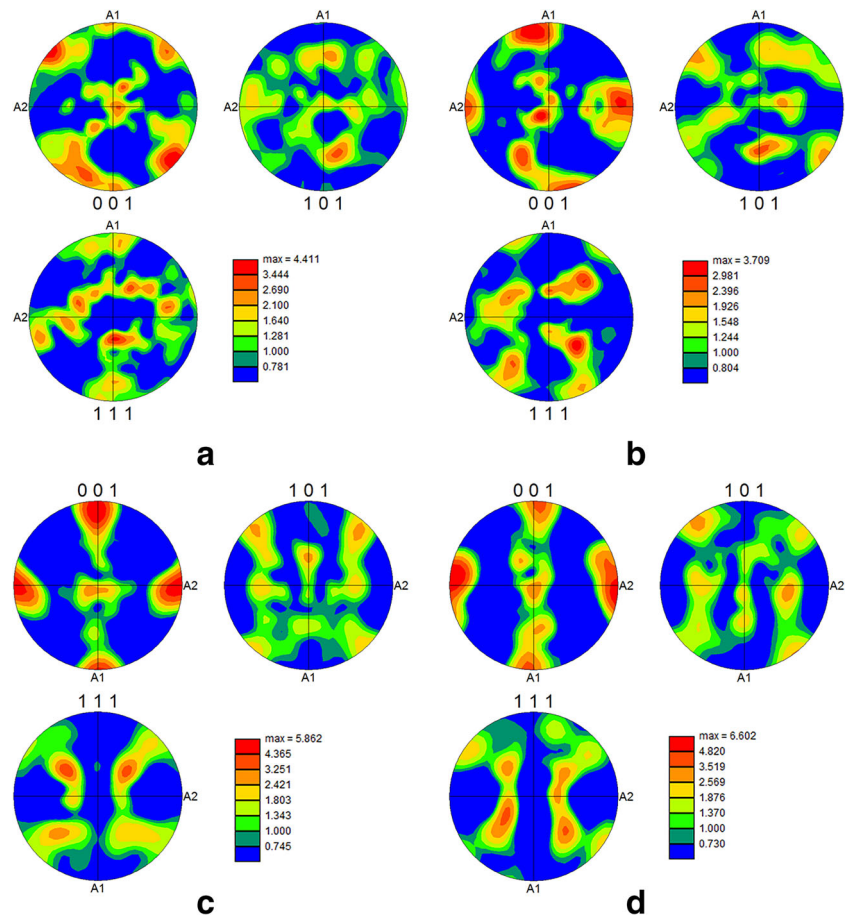


Fig. 5 Comparison of average grain size obtained in the four cases

Grain texture The texture of the fusion zone obtained by EBSD can be assessed using (001), (101) and (111) pole figures, obtained for the four different heat inputs (see Fig. 6). A1 and A2 are the y- and x-axes of the projection surface. The colors indicate the intensity normalized to the random background. In the 87.5–120 J/mm heat input range, the texture is board-like, especially at 75 J/mm: all three 100 poles are aligned. Such alignment predetermines the texture observed in the (111) and (110) pole figures. The transition from the board texture to fiber texture is shown in Fig. 6c.

The strongest texture was obtained at 58 J/mm heat input: it is symmetrical in the y-direction and very intense in the x-direction (see Fig. 6d). The texture of the sample completely changed from the board-like to the fiber one.

Fig. 6 Pole figure obtained for the heat inputs **a** 120 J/mm, **b** 87.5 J/mm, **c** 75 J/mm and **d** 58 J/mm



The juxtaposition of experimental and theoretical results showed that the pole figures can provide more information if combined with the EBSD data [25, 26] (see Fig. 7). 64.4% of the crystals, their $\langle 001 \rangle$ orientations point to the A1 direction. Almost all of these grains are columnar ones, which agrees with corresponding pole figure. It is indicated that in the weld consist entirely of straight columnar grain, the preferential growth direction of grains is almost the same as the actual growth direction of columnar grains. The strong texture may lead to a totally anisotropic joint. While in the weld consist of curved columnar grains, the preferential growth direction and the actual growth direction of grains are only identical at the beginning of grain growth. There is no obvious texture formation in curved columnar grains weld. The equiaxed grains show a totally random direction which may lead to an isotropic joint.

4 Conclusion

The grain structure and topology in laser-welded Al alloy was analyzed numerically and experimentally. The macroscopic simulation provided welding pool geometries

while the mesoscopic modeling offered insights on the grain structure evolution. Both theoretical analyses were verified experimentally. Influence of heat input on the grain structure evolution was studied in detail, and the following conclusions were obtained.

1. The difference in the heat flux distribution results in different molten pool shapes and, as a result, affects solidification boundary morphology. The growth of the columnar grains is perpendicular to the solidification boundary of the molten pool along the temperature gradient. The morphology of the columnar grains changes from the curved to straight ones as the heat inputs decrease.
2. Decreased welding heat input reduces the peak temperature and real-time residence time. As a result, columnar grains become smaller. There is an abnormal rise in columnar grain size when the grain morphology is on the stage of transition from curved to straight.
3. The mushy zone of the solidification boundary of the molten pool strongly affects the formation of the equiaxed grains. The larger the ratio of the mushy zone area to that of the corresponding molten pool, the easier

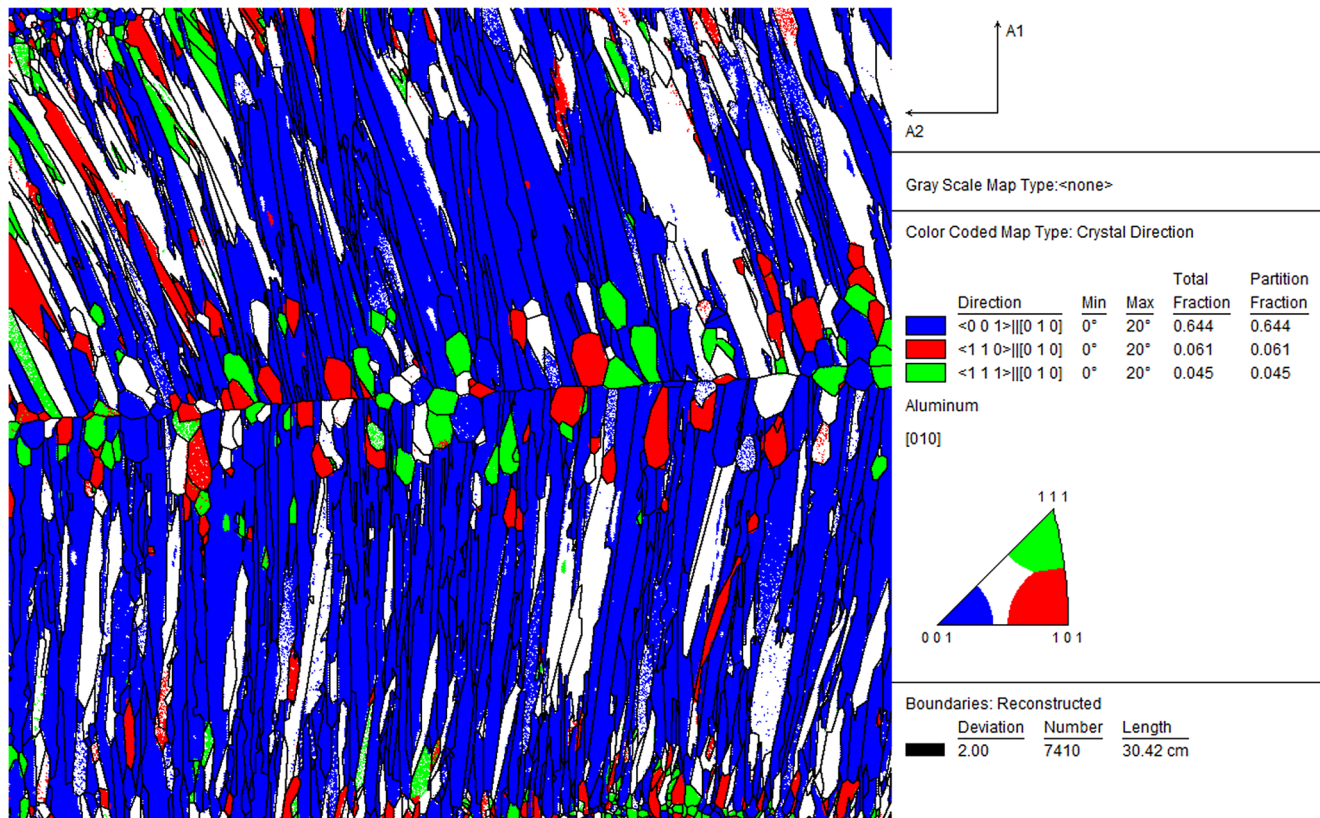


Fig. 7 EBSD map of the weld. Grains colored in blue, red and green are the $\langle 001 \rangle$, $\langle 101 \rangle$ and $\langle 111 \rangle$ orientations within a 20° angle relative to the A1 direction, respectively

it is for the equiaxed grains to nucleate and grow. Formation and presence of these equiaxed grains will hinder columnar grain growth.

- As the heat input decreases, the board texture of the weld transforms into a fibrous texture.

Funding This work received support from the National Natural Science Foundation of China through Grant (No. 51105049).

References

- Zhao H, White DR, DebRoy T (1999) Current issues and problems in laser welding of automotive aluminium alloys. *Int Mater Rev* 44(6):238–266
- Matsuda F, Hashimoto T, Senda T (1969) *Trans Natl Res Inst Mete (Jpn)* 11(1):83
- Davies GJ, Garland JG (1975) Solidification structures and properties of fusion welds. *Int Met Rev* 20:83–105
- Savage WF (1980) Solidification, segregation, imperfections, weld. *World* 18:89
- Chen SJ, Guillemot G, Gandin C-A (2016) Three-dimensional cellular automaton-finite element modeling of solidification grain structures for arc-welding processes. *Acta Mater* 115:448–467
- Wei YH, Zhan XH, Dong ZB et al (2007) Numerical simulation of columnar dendritic grain growth during weld solidification process. *Sci Tech Weld Join* 12(2):138–146
- Mishra S, DebRoy T (2006) Non-isothermal grain growth in metals and alloys. *J Mater Sci Tech* 22(3):253–278
- Wei HL, Elmer JW, DebRoy T (2017) Crystal growth during keyhole mode laser welding. *Acta Mater* 133:10–20
- Rodgers TM, Mitchell JA, Tikare VA (2017) Monte Carlo model for 3D grain evolution during welding. *Model Simul Sci Eng* 25(6):064006
- Kang Y, Zhan XH, Qi CQ et al (2019) Grain growth and texture evolution of weld seam during solidification in laser beam deep penetration welding of 2219 aluminum alloy. *Mater Res Express* 6(11):1165e3
- Farzadi A, Serajzadeh S, Kokabi AH (2008) Modeling of heat transfer and fluid flow during gas tungsten arc welding of commercial pure aluminum. *Int J Adv Manuf Technol* 38:258–267
- Geng SN, Jiang P, Guo LY et al (2020) Multi-scale simulation of grain/sub-grain structure evolution during solidification in laser welding of aluminum alloys. *Int J Heat Mass Transf* 119252:149
- Chen C, Lin YJ, Ou H et al (2018) Study of heat source calibration and modelling for laser welding process. *Int J Precis Eng Manuf* 19(8):1239–1244
- Rodgers TM, Madisonb JD, Tikarec V (2017) Simulation of metal additive manufacturing microstructures using kinetic Monte Carlo. *Comp Mater Sci* 135:78–79
- Gao J, Thompson RG (1996) Real time-temperature models for Monte Carlo simulations of normal grain growth. *Acta Mater* 44(11):4565–4570
- Wei HL, Elmer JW, DebRoy T (2017) Three-dimensional modeling of grain structure evolution during welding of an aluminum alloy. *Acta Mater* 126:413–425

17. Mitchell JA, Tikare V (2016) A model for grain growth during welding. Sandia National laboratory(US) SAND2016-11070
18. Plimpton S, Battaile C, Chandross M et al (2009) Crossing the mesoscale no-man's land via parallel kinetic Monte Carlo. Sandia National Laboratory(US), SAND2009-6226. <http://spparks.sandia.gov>
19. Garcia AL, Tikare V, Holm EA (2008) Three-dimensional simulation of grain growth in a thermal gradient with non-uniform grain boundary mobility. *Scripta Mater* 59(6):661–664
20. Mishra S (2003) Grain growth in the heat-affected zone of Ti-6Al-4V alloy welds: measurements and MC simulations[*master's thesis*]. The Pennsylvania State University, Pittsburgh PA
21. Wei HL, Knapp GL, Mukherjee T et al (2019) Three-dimensional grain growth during multi-layer printing of a nickel-based alloy Inconel 718. *Addit Manuf* 25:448–459
22. Kou S (2003) *Welding metallurgy*. 2nd ed. Chapter 7, Weld metal solidification I: Grain structure,170-178, Wiley & Sons Inc., New Jersey(US)
23. Bolzoni L, Xia M, Babu NH (2016) Formation of equiaxed crystal structures in directionally solidified Al-Si alloys using Nb-based heterogeneous nuclei. *Sci Reports* 6:39554
24. Lippold JC (2015) *Welding metallurgy and weldability*,18-30, John Wiley & Sons Inc., New Jersey(US)
25. Hector LG, Chen YL, Agarwal S et al (2004) Texture characterization of autogenous Nd:YAG laser welds in AA5182-o and AA6111-t4 aluminum alloys. *Metall Mater Trans A* 35(9):3032–3038
26. Boumerzoug Z, Chérifi N, Baudin T (2014) Texture in welded industrial aluminum. *Mech Mater* 563:7–12

Publisher's note Springer Nature remains neutral with regard to jurisdictional claims in published maps and institutional affiliations.